DOI 10.1007/s11141-015-9561-x
Radiophysics and Quantum Electronics, Vol. 57, No. 10, March, 2015
(Russian Original Vol. 57, No. 10, October, 2014)

SYNCHRONIZATION IN THE SYSTEM OF SYNAPTICALLY COUPLED NEURAL OSCILLATORS WITH FREQUENCY-DEPENDENT COUPLING

I. S. Prokin[1,2] **and V. B. Kazantsev**[1,2*]

UDC 534.1

We study the influence of the frequency-dependent coupling on synchronization in a model system of the synaptically coupled neural oscillators is studied. The ranges of parameters for which the locking of the frequency of the driven (output) neural oscillator is observed are obtained. The phase characteristics of oscillations in the synchronization regime are studied. The phase mappings are numerically plotted to describe the above-mentioned characteristics and analytical estimates for these mappings are obtained for certain restrictions imposed on the frequency characteristics of the oscillators. The effect of the frequency-dependent variation in the coupling is shown to lead to a substantial change (narrowing) of the synchronization regions compared with the case of fixed synaptic coupling.

1. INTRODUCTION

The study of the dynamical mechanisms of the electrochemical-signal transmission in the brain is referred to key fundamental problems of modern science. It is known in biophysics that the nerve cells (neurons) of the brain are capable of generating the pulsed activity signals (spikes) of electrochemical nature and send them to other neurons by synaptic couplings. Synaptic coupling is die to extraction of special chemical substances (neuromediators) by a transmitting (presynaptic or input) cell and detection of the above substances by a receiving (postsynaptic or output) cell. Therefore, the neural activity depends on both the intrinsic current state of the neuron and the state of other neurons influencing the above neuron, as well as on the properties of the synaptic couplings which are formed by the above neuron with the neighboring neurons.

The problem of studying the dynamics of the transmitting neuron–synapse–receiving neuron system can be treated as a problem of oscillations of the neural oscillator under the action of an external pulsed force. The studies of synchronization in neural systems have been described in sufficiently many papers [1–13]. In the majority of the classical works, the complex dynamics of the neural-oscillator response is usually associated with the complex nature of the own dynamics of neurons, which, depending on their type, can possess various periodic, quasi-periodic, and chaotic regimes [14–16] even without external actions. Under certain conditions, forcing by an external periodic signal can lead to forced neuron synchronization. In neurobiology, the effect of synchronization of the neurons in various parts of the brain is considered to be a basic phenomenon that is related to the sensor-information processing, associated perception, and motor coordination, as well as various pathologic alterations, for example, epileptiform activity [17–24].

Recent studies have shown that along with the complex dynamics of the neurons themselves, synaptic coupling can play an important role in the formation of the information functions due to the so-called

* vkazan@neuron.appl.sci-nnov.ru

[1] N. I. Lobachevsky State University of Nizhny Novgorod; [2] Institute of Applied Physics of the Russian Academy of Sciences, Nizhny Novgorod, Russia. Translated from Izvestiya Vysshikh Uchebnykh Zavedenii, Radiofizika, Vol. 57, No. 10, pp. 834–848, October 2014. Original article submitted May 20, 2013; accepted October 2, 2014.

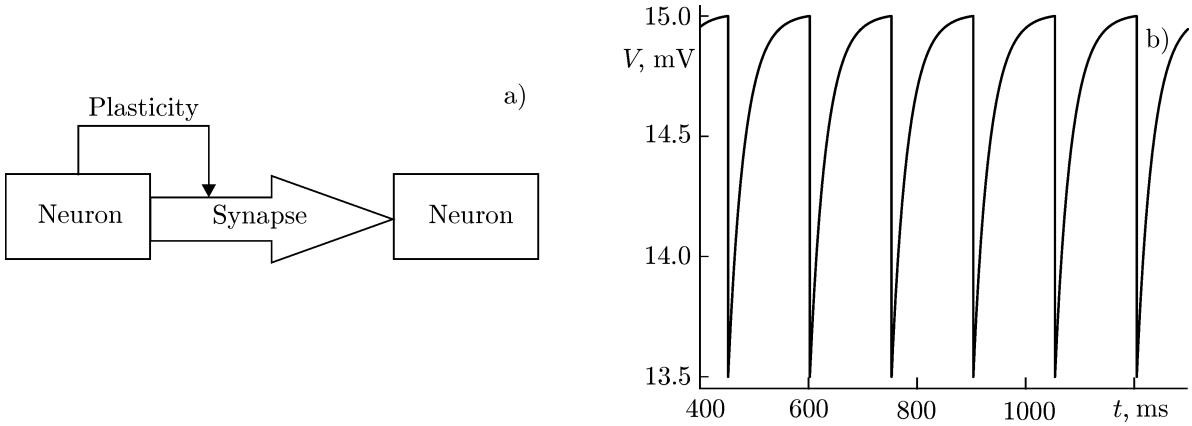

Fig. 1. Model diagram (*a*) and oscillations in the neuron model for $V_{\rm b} = 15.01$ mV (*b*).

synaptic plasticity. The synaptic plasticity of the interneuron couplings is a dynamical variation in the coupling force as a function of the characteristics of signals of the coupled neurons (in particular, the presynaptic (input) neuron). The short-term plasticity, i.e., coupling-force variation as a function of the pulse-repetition rate, is one of the well-known plasticity forms. The coupling strengthening/weakening for this plasticity form is observed at the millisecond scale and related to a change in the secretion value of a neuromediator (chemical substance participating in synaptic transmission from the transmitting neuron to the receiving one) in a presynaptic ending. Therefore, when analyzing the neural oscillator response to the external pulsed signal, one should take into account that the external-force amplitude becomes a function of the external-signal frequency.

The model of two synaptically coupled neural oscillators with the simplest intrinsic dynamics but with the frequency-dependent coupling was considered in [25]. Using the analysis of nonlinear point mappings, the description of various configurations of the response of the driven neural oscillator is obtained in [25] in the case where the forced-oscillation regime is realized. In this regime, a significant difference in the parameter-space partitioning with allowance for the frequency-dependent coupling was revealed. In addition, a possibility of realizing complex response configurations ensured by the dynamical nature of interaction is established for some values of the model parameters.

In this work, we continue to study the plasticity influence on the coupled-oscillator dynamics in the case of oscillation synchronization, as well as the realization of different regimes of locking the phase of the periodic pulse signal generated by an input oscillator compared with fixed nonplastic coupling.

2. THE MODEL

Let us consider the following model of the neural oscillator [25, 26]:

$$\tau \frac{{\rm d}V}{{\rm d}t} = -V + V_{\rm syn} + V_{\rm b} \tag{1a}$$

for $V(t) \le V_{\rm thr}$ and

$$V(t+0) = V_{\rm reset} \tag{1b}$$

for $V(t) = V_{\rm thr}$. Here, the variable V qualitatively describes the membrane potential of the neuron, $V_{\rm syn}$ is the potential formed due to the input synaptic actions, $V_{\rm b}$ is the depolarization parameter (which determines the dynamical regime of the neuron in the absence of the input signals at the synapses), τ is the typical relaxation time, $V_{\rm thr}$ is the threshold level of the potential, $V_{\rm reset}$ is the reset level, and t is the time. We use t_k to denote the time instants at which the membrane potential reaches the threshold. The model diagram and the typical form of oscillations are shown in Fig. 1.

To describe the dynamics of the frequency-dependent plastic synapse, we rewrite the system of equations in [27], grouping the equations for the variables which describe the synapse and explicitly singling out the pulse-appearance instants:

$$\frac{\mathrm{d}x}{\mathrm{d}t} = \frac{z}{\tau_{\mathrm{rec}}} - \sum_{k=1}^{N} ux\delta(t-t_k), \qquad \frac{\mathrm{d}y}{\mathrm{d}t} = -\frac{y}{\tau_1} + \sum_{k=1}^{N} ux\delta(t-t_k),$$
$$\frac{\mathrm{d}z}{\mathrm{d}t} = \frac{y}{\tau_1} - \frac{z}{\tau_{\mathrm{rec}}}, \qquad \frac{\mathrm{d}u}{\mathrm{d}t} = -\frac{u}{\tau_{\mathrm{fac}}} + \sum_{k=1}^{N} U\,(1-u)\,\delta(t-t_k). \tag{2}$$

Here, x, y, and z are the variables describing the shares of the synaptic resources in the recovered, active, and inactive states, respectively, u is the variable responsible for the frequency-dependent strengthening/suppression of the synaptic coupling, and τ_{rec}, τ_1, and τ_{fac} are typical times of the synapse dynamics. The phenomenological variables of the model can have the following meaning: x is the neuromediator quantity in a presynaptic ending, which is ready to be ejected to the synaptic cleft; y is the quantity proportional to the share of open postsynaptic channels; z is the number of the synthesized neuromediator, which is not ready to be ejected to the synaptic cleft (in the presynaptic ending); u is the quantity proportional to the probability of the neuromediator release from the presynaptic ending; the parameter U describes variation in u due to the presynaptic spike.

Each input pulse leads to a jump in the variable y after which this variable drops to zero for a comparatively short time. For the used the model parameters, the jump of the variable y decreases with each subsequent input pulse if the interval between the input pulses is not sufficiently large for the synapse to recover to the initial state. Therefore, the coupling force decreases stronger and faster with increasing input-pulse rate. In this case, the stationary value of the jumps is determined by the nonlinear function of the input-action frequency for a periodic input action [25].

The synaptic coupling between the input and output neural oscillators (each oscillator is described by Eq. (1)) is ensured by the weighted variable y:

$$V_{\mathrm{syn}} = Ay(t),$$

where A is the coupling weight.

To describe the synaptic coupling in a model with fixed coupling, the variable y is redefined as follows:

$$V_{\mathrm{syn}} = Ay(t) = M\sum_{k=1}^{N}\delta(t-t_k),$$

where M is a certain normalization constant. Note that the constant M is chosen such that an increase in the potential V due to the action of a single input pulse is the same for the model with frequency-dependent coupling and initial conditions $V(0) = V_{\mathrm{b}}$, $x(0) = 1$, and $y(0) = z(0) = u(0) = 0$ and the model with fixed coupling and initial conditions $V(0) = V_{\mathrm{b}}$ [25]:

$$AU\frac{\tau_1}{\tau_1-\tau}\left[\left(\frac{\tau}{\tau_1}\right)^{\frac{\tau}{\tau-\tau_1}} - \left(\frac{\tau}{\tau_1}\right)^{\frac{\tau_1}{\tau-\tau_1}}\right] = \frac{M}{\tau}.$$

3. ANALYSIS OF THE MODEL IN THE SYNCHRONIZATION REGIME

Consider the case where the input oscillator operates in the self-oscillating regime and generates a periodic sequence of pulses. In this case, the oscillation frequency f_{in} is determined by the depolarization parameter.

Periodic pulses of the input oscillator specify a sequence of the temporal secants which determine the

stroboscopic mapping for the membrane potential of the output neuron in the extended system. To analyze the synchronization regimes from the convenience viewpoint, we use a parameter similar to the quantity that is a reciprocal of the rotation number in the classical theory of oscillations [28]. We define this parameter as $m = f_{\text{in}}/f_{\text{out}}$, where f_{out} is the realization-averaged rate of the output pulse sequence (in the numerical calculation, the realization length was chosen such that to keep the input-pulse number constant and equal to 100). The convenience of the parameter m is that it takes integer values in the presence of the frequency locking in the model.

If the realization length tends to infinity when calculating the parameter m, the latter takes its limiting value L. The rational values of $L = p/q$ indicate the frequency locking, i.e., $pf_{\text{out}} = qf_{\text{in}}$, while the irrational values of L testify to asynchronous dynamics. An infinitely large L indicates the absence of response.

The parameter m can be used for estimating the synchronization regimes in the case $V_{\text{b}} > V_{\text{thr}}$ where the output neuron is in the oscillatory mode and in the case of forced oscillations (the output neuron is in the excitable mode $V_{\text{b}} < V_{\text{thr}}$).

To analyze the phase dynamics, we introduce the phase of the ith pulse of the output signal with respect to the periodic input signal as $\Psi_i = \{t_i f_{\text{in}}\}$, where the braces denote the operator of taking the fractional part. In other words, Ψ_i is the time between the ith pulse of the response and the nearest previous input pulse, which is normalized to the repetition period of the input pulses. The pulse phase determined in such a way takes the values from the half-open interval $[0; 1)$ so that zero corresponds to the in-phase arrival of the pulse with respect to the periodic input signal, while $1/2$ corresponds to the antiphase arrival.

To estimate the regimes of the phase locking and the phase synchronization in the numerical experiment, we use the realization-averaged phase $\langle\Psi\rangle$ and the standard deviation $\text{std}(\Psi)$ from the average for the realization. The small standard deviation ($\text{std}(\Psi) \ll \langle\Psi\rangle$) indicates phase locking.

Division of the plane section of the parameter space (A, V_{b}, f_{in}) into the regions of different configurations of the response is shown in Fig. 2. The regions with the phase scattering value in the vicinity of zero correspond to the regions of the frequency locking with the integer values of the locking parameter m and the regions of maximum phase scattering correspond to the regimes of generation of complex pulse sequences.

Note that the synchronization regions (black regions in Figs. 2*e* and 2*f*) have the shape of "tongues" (the Arnold tongues) with the vertices at the points of multiple ratios of the input-oscillator ("forcing") frequency and the eigenfrequency of oscillations of the output oscillator, which corresponds to the classical theory of synchronization [29–31]. It should also be noted that the form of these regions is significantly different for the model with fixed coupling (Figs. 2*a*, 3*c*, and 2*e*) and the model with plastic coupling (Figs. 2*b*, 2*d*, and 2*f*) with increasing forcing amplitude (coupling coefficient). In the case of plastic coupling, the regions are narrow and localized in the vicinity of the multiple values of frequencies for sufficiently large forcing amplitudes. This effect can be explained by that the phase is locked for the effectively higher values of the coupling weight A due to the frequency-dependent weakening of the coupling (variable $y(t)$). This significantly narrows the synchronization regions and allows one to interpret the frequency-dependent plasticity of the couplings as a possible mechanism of selective response and contrasting the frequency-coded information in the brain.

To analyze the phase dynamics and bifurcation mechanisms of the phase locking, we consider the phase mappings of the following types

$$T\colon \Psi_i \to \Psi_{i+1}, \qquad i \in \mathbb{N},$$

where $\mathbb{N}$ is the set of the natural numbers $1, 2, 3, \ldots$. The mapping relates the phase Ψ_i at the time of the ith pulse of the response to the phase Ψ_{i+1} at the time of the $(i+1)$st pulse of the response.

We first consider the case of fixed coupling. A good example of plotting the mappings for the model of oscillators of the threshold integrator type, which are coupled by the fixed bidirectional coupling, is shown

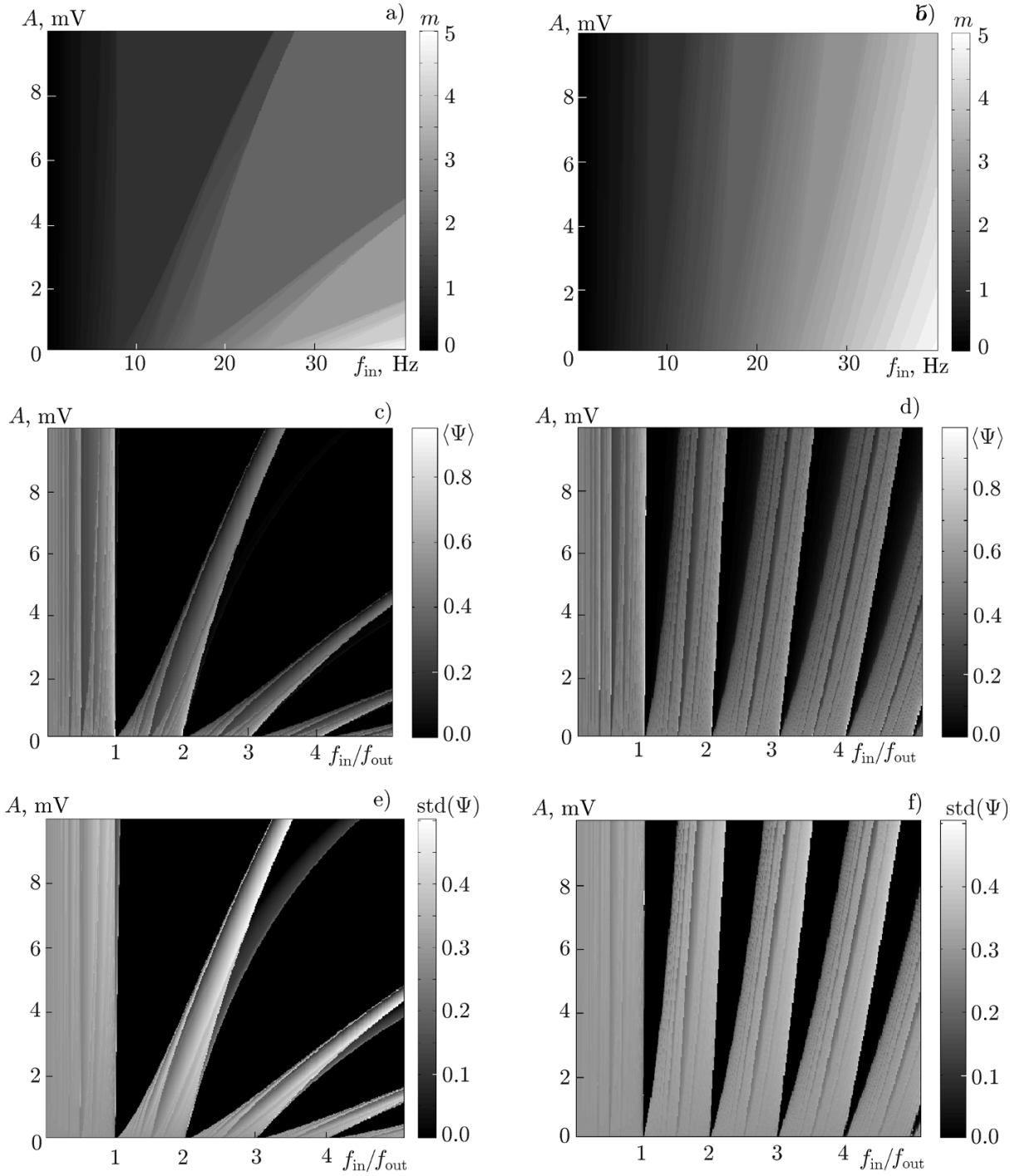

Fig. 2. Division of the plane section of the parameter space into the regions of different configurations of the response for the model with fixed *a*) and frequency-dependent plastic (*b*) coupling. Parameter $V_{\text{b}} = 15.021$ mV corresponds to the pulse frequency $\Phi = 7.78$ Hz in the absence of the input signal, i.e., the frequency of the autonomous output oscillator.

in [32] for the special case where the eigenfrequencies are identical. Note that if we ensure the condition $\Phi\Delta t > 1$, where Φ is the eigenfrequency of the output oscillator (the pulse-repetition rate in the absence of external action), which is expressed via the parameter V_{b}, and $\Delta t = 1/f_{\text{in}}$ is the interpulse interval of the input oscillator, then the composite mapping of the output-pulse times can be obtained. This mapping is analytically represented in the form

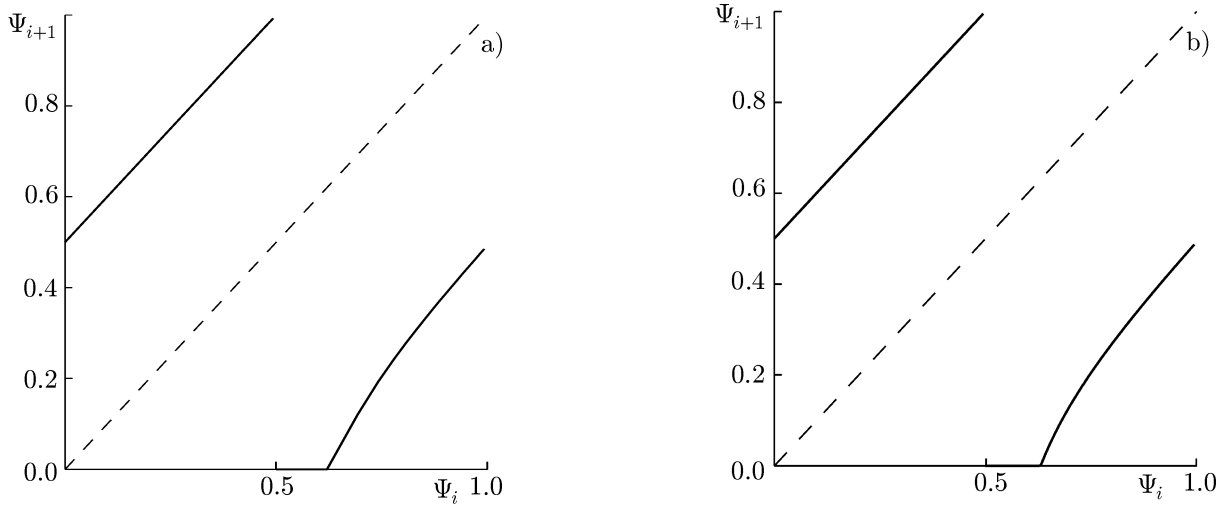

Fig. 3. The numerically (*a*) and analytically (*b*) obtained first return functions for the phase mappings. The parameters are equal to $h = 0.05$ ms, $A = 2$ mV, $V_{\rm b} = 15.0555$ mV ($\Phi = 10$ Hz), and $f_{\rm in} = 5$ Hz, and h is the integration step of analytical solutions of the differential equations.

$$t_{i+1} = Z(t_i) = \begin{cases} t_i + 1/\Phi - S[\eta(n) - t_i], & \exists n \in \mathbb{N}_0 \colon \eta(n) \in (t_i; \xi); \\ \eta(k = n), & \exists n \in \mathbb{N}_0 \colon \eta(n) \in [\xi; t_i + 1/\Phi); \\ t_i + 1/\Phi, & \nexists n \in \mathbb{N}_0 \colon \eta(n) \in (t_i; t_i + 1/\Phi). \end{cases}$$

Here,

$$S(x) = -\tau \ln\left[1 + \frac{M}{\tau\,(V_{\rm reset} - V_{\rm b})\,\exp(-x/\tau)}\right]$$

is the function of the output-pulse shift,

$$\xi = -\tau \ln\left[\exp\big(-\frac{1}{\Phi\tau}\big) - \frac{M}{\tau\,(V_{\rm reset} - V_{\rm b})}\right]$$

is the time during which the output oscillator exponentially evolving from the reset level critically approaches the threshold (so that the input-oscillator pulse instantly gives rise to the response pulse), $\eta(k) = t_{\rm pre0} + k\,\Delta t$ is the function determining the input-pulse times, $t_{\rm pre0}$ is the time of appearance of the first input pulse in the considered realization, $k \in \mathbb{N}_0$ is the number of the input-oscillator pulse, and $\mathbb{N}_0 = \{0; 1; 2; \dots\}$ is the set of natural numbers with zero. Since the pulse times uniquely determine the phase $\Psi_i = \{t_i f_{\rm in}\}$, the time mapping uniquely determines the phase mapping.

Figure 3 shows the typical behavior of the first return function for the phase mapping in the case of fixed coupling. In this case, the phase performs periodic oscillations between two mapping branches.

In the general case, analytical construction of the phase mapping is difficult. Therefore, in what follows, numerical calculation of the first return function will be used to analyze the dynamical regimes and bifurcation transitions.

The stable fixed point of the phase mapping corresponds to the phase locking. An example for the parameter values for the locking region, which corresponds to the regime $1 : 1$ ($m = 1$), is shown in Fig. 4*b*. Figure 4*c* demonstrates the corresponding normalized realizations for the membrane potential. The above example shows that during the mapping iterations for any initial conditions the phase asymptotically approaches its fixed point in the vicinity of zero. An example of the first return function for the phase mapping is given in Fig. 5 for the region dividing the locking regions $1 : 1$ and $2 : 1$. In this case, the mapping has no fixed points, which manifests itself in the oscillations of the pulse phases during realization.

Note that similarity of the two considered models (see Fig. 2), which become indistinguishable for

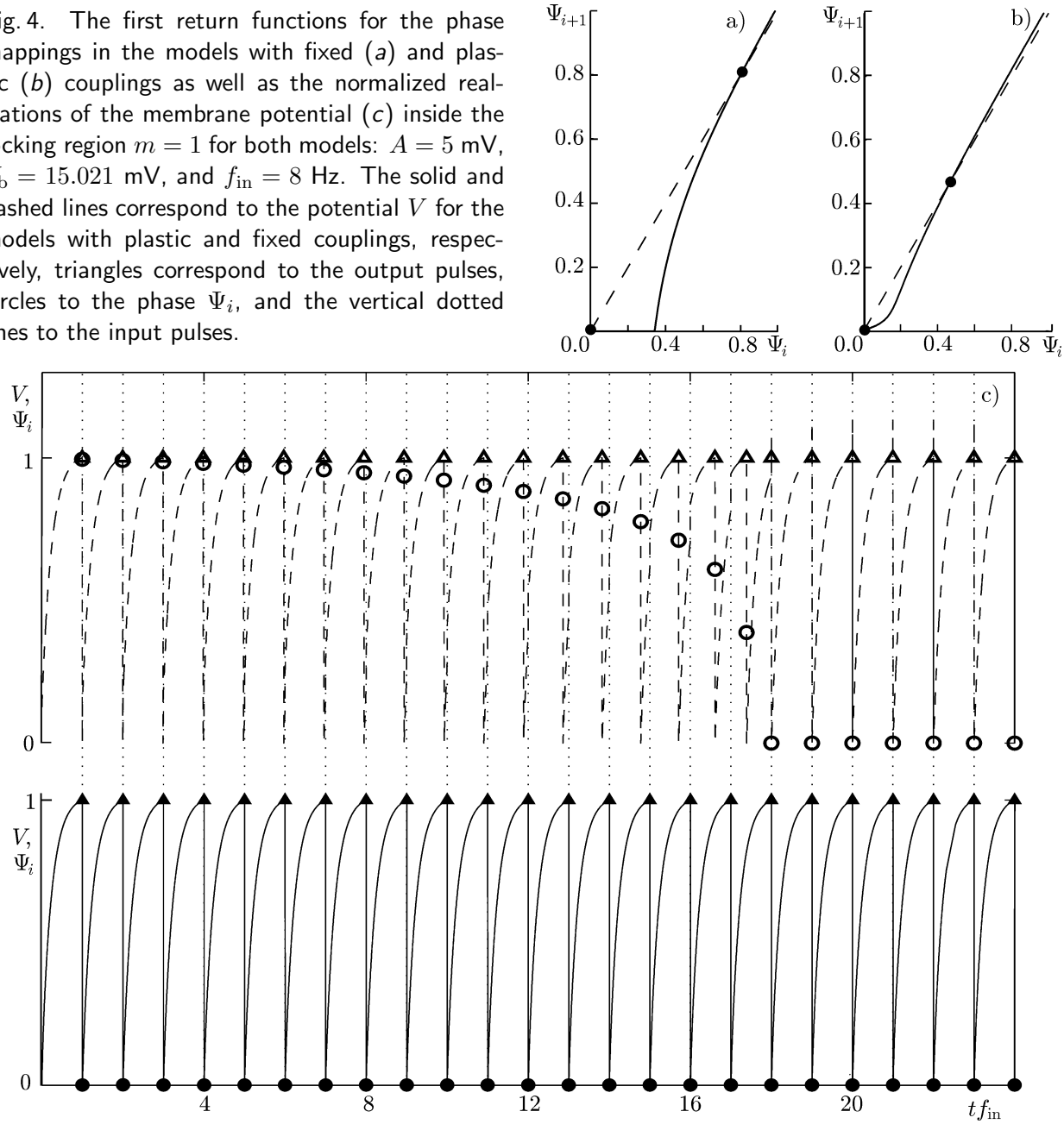

Fig. 4. The first return functions for the phase mappings in the models with fixed (a) and plastic (b) couplings as well as the normalized realizations of the membrane potential (c) inside the locking region $m = 1$ for both models: $A = 5$ mV, $V_{\text{b}} = 15.021$ mV, and $f_{\text{in}} = 8$ Hz. The solid and dashed lines correspond to the potential V for the models with plastic and fixed couplings, respectively, triangles correspond to the output pulses, circles to the phase Ψ_i, and the vertical dotted lines to the input pulses.

an infinitesimally small coupling coefficient (see Figs. 6 and 7), increases with decreasing coupling force (coefficient A).

Consider the cases of boundaries of the region $m = 1$ in more detail. The region $m = 1$ in the model with plastic coupling for the parameters $A = 2$ mV and $V_{\text{b}} = 15.021$ mV is specified by the inequalities 7.8005 Hz$< f_{\text{in}} <$ 9.661 Hz, while in the model with fixed coupling we have 7.7701 Hz$< f_{\text{in}} <$ 12.1506 Hz (the boundaries are determined numerically with indicated accuracy).

It is evident from Fig. 8b that if the parameters are below the lower boundary of the region $m = 1$, then the phase decreases slowly or rapidly with a large or small delay of the response pulse from the preceding input pulse, respectively. According to Figs. 8c and 8d and Figs. 5a and 5 c, if the parameters are higher than the upper boundary of the region $m = 1$, then the exit from the synchronization regime occurs in the opposite manner, i.e., the phase increases slowly or rapidly for a small or large delay, respectively. Note that the two considered models are qualitatively similar with respect to exit from the synchronization regime, which is well demonstrated in the bifurcation diagram for fixed points of the phase mapping.

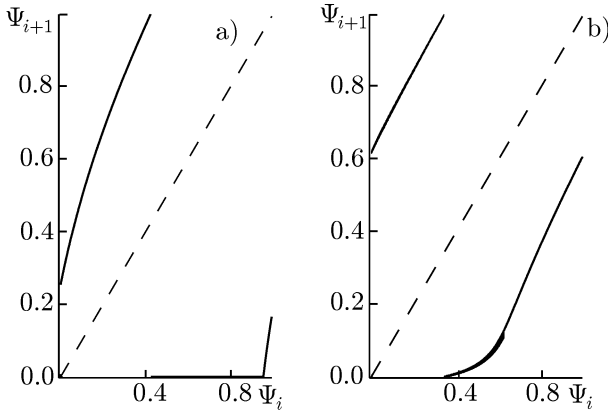

Fig. 5. The same as in Fig. 4, but for the parameters outside (above) the locking region $m = 1$ for both models: $A = 2$ mV, $V_{\rm b} = 15.021$ mV, and $f_{\rm in} = 13$ Hz.

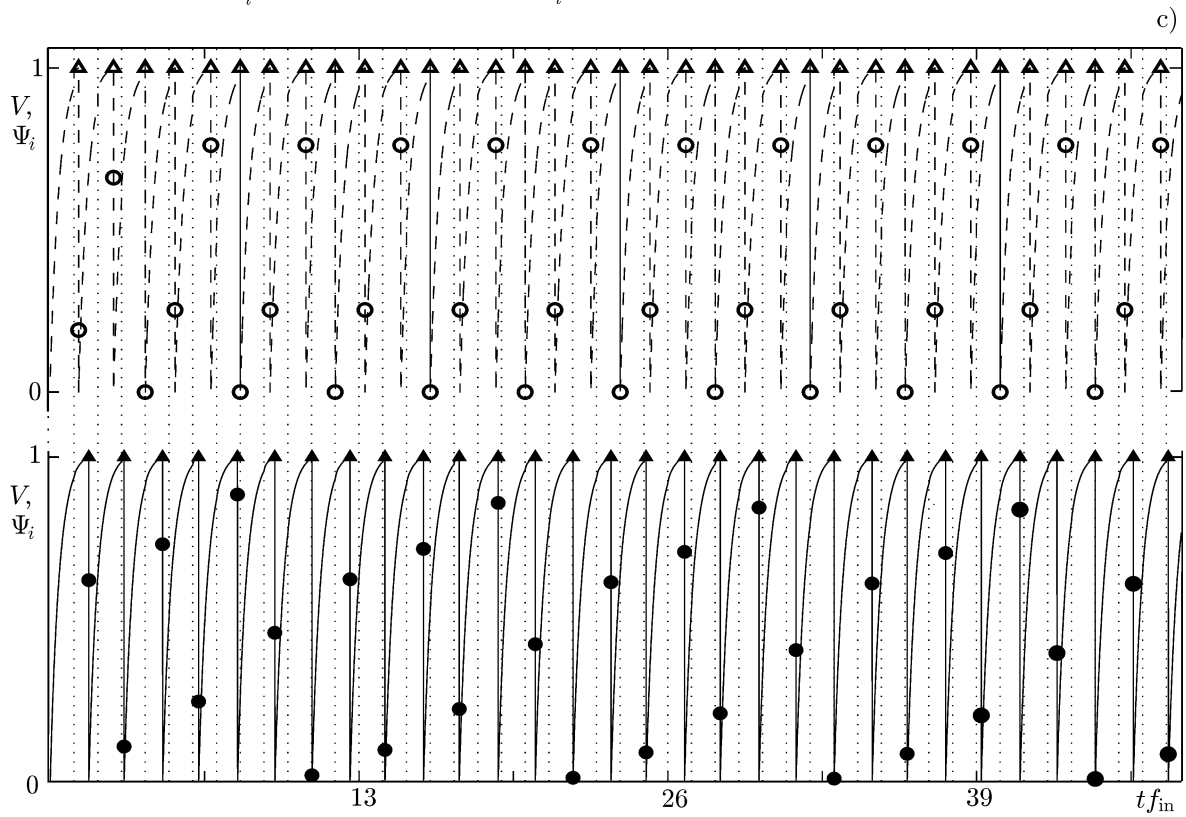

Figures 9*a* and 9*b* show the bifurcation diagram for the fixed points of the phase mapping in the frequency range that covers the locking region $m = 1$. This diagram illustrates coincidence of the bifurcation mechanisms of the phase mapping, which describe the synchronization appearance/disappearance in the models with fixed (Fig. 9*a*) and plastic (Fig. 9*b*) couplings. In both cases, the saddle-nodal bifurcations occur on the left- and right-hand boundaries of the phase-mapping region. Figure. 9*c* schematically illustrates the circumference-mapping dynamics with increasing input frequency. The open and close circles in Fig. 9*c* denote the unstable and stable fixed points, respectively. The arrows on the circumference denote the phase-variation direction for a small deviation from the fixed points. The arcs with the arrows above the circumference denote displacement of the fixed points with respect to the zero phase with the variation in the bifurcation parameter, i.e., input frequency. The locking-region boundaries in both models have a structurally unstable fixed saddle-node point which loses its stability with a small frequency variation.

It should be noted that for the frequencies corresponding to the region $m = 1$ in the model with the plastic coupling, the fixed-point coordinate is a function of frequency, whereas this effect is not observed in the model with fixed coupling.

To describe the pulse-phase dynamics in the case where the relationship $f_{\rm out} < f_{\rm in}$ takes place, we

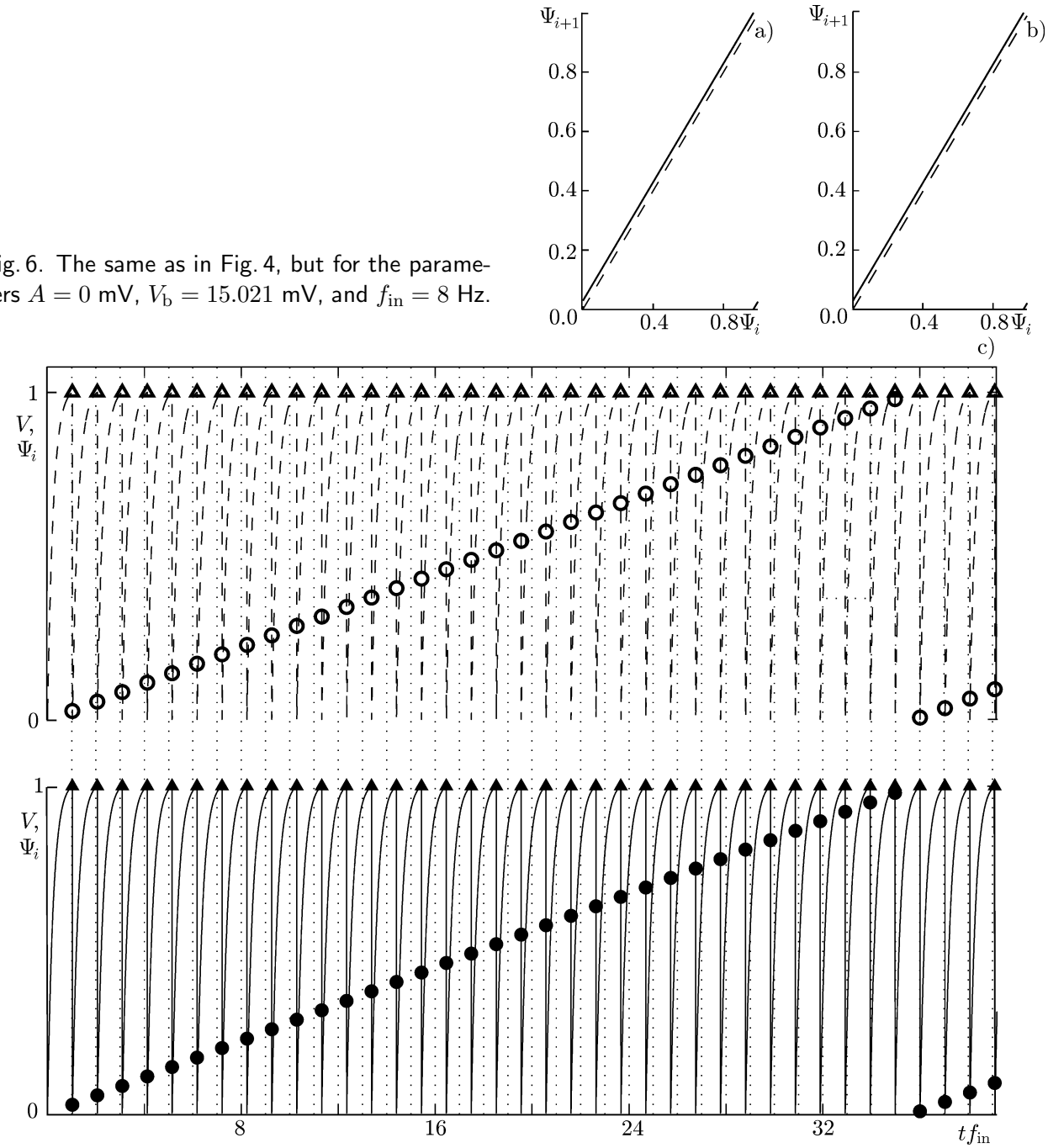

Fig. 6. The same as in Fig. 4, but for the parameters $A = 0$ mV, $V_{\text{b}} = 15.021$ mV, and $f_{\text{in}} = 8$ Hz.

introduce the phase parameter

$$\Theta_1 = \{t_1 f_{\text{in}}\}, \qquad \Theta_i = t_i f_{\text{in}} - [t_{i-1} f_{\text{in}}] - 1, \qquad i = 2, 3, \ldots,$$

where $[x]$ is the operator of taking the integer part of the number x.

The integer part of the introduced parameter determines the number of the input pulses preceding this output pulse. It is noteworthy that the fractional part of the phase parameter Θ_i is identical to the previously determined pulse phase Ψ_i. By implication, the relationship between the parameter m and the quantity $[\Theta_i]+1$ is similar to the relationship between the average and instantaneous velocities in kinematics.

Consider the dynamics of the "instantaneous phases" on the bifurcation diagram for the realization. Such a diagram is constructed as follows. The setting of the stationary regime for various frequency values of the input pulse sequence is expected during 100 periods of the input pulse sequence and then the phases

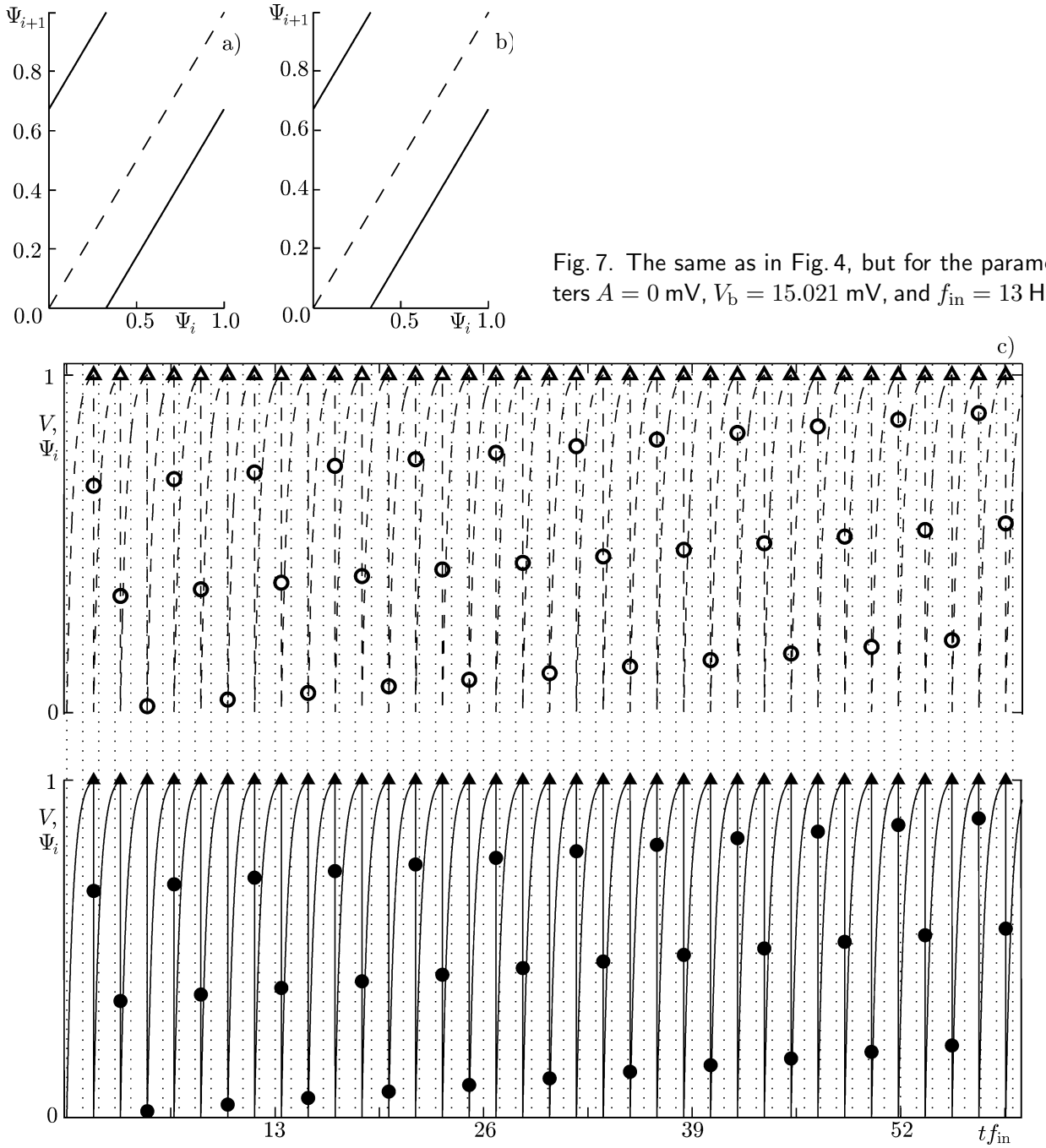

Fig. 7. The same as in Fig. 4, but for the parameters $A = 0$ mV, $V_{\text{b}} = 15.021$ mV, and $f_{\text{in}} = 13$ Hz.

of 1000 subsequent input pulses are calculated.

The examples of such diagrams are given in Figs. 10 and 11 for $A = 2$ mV and $V_{\text{b}} = 15.021$ mV for the phase characteristics Θ_i and Ψ_i, respectively.

In the plots of $[\Theta](f_{\text{in}})$ for both models, with plastic (Fig. 10*d*) and fixed (Fig. 10*c*) couplings, one can see the regions where the pulses with the neighboring integer values of this characteristic coexist, as well as the regions where all interpulse intervals for the output pulse sequence have the same number $[\Theta]+1$ of input pulses. When choosing parameters inside the synchronization regions in the model with plastic coupling, the fixed-point coordinate depends on the frequency (Fig. 11*b*), which determines various phase delays of the output pulse with respect to the input one. We also note the synchronization absence at high frequencies in the model with the plastic coupling (Fig. 8*d*) due to the dynamical weakening of the coupling, which leads to a sharp decrease in the effective force of the coupling with increasing frequency.

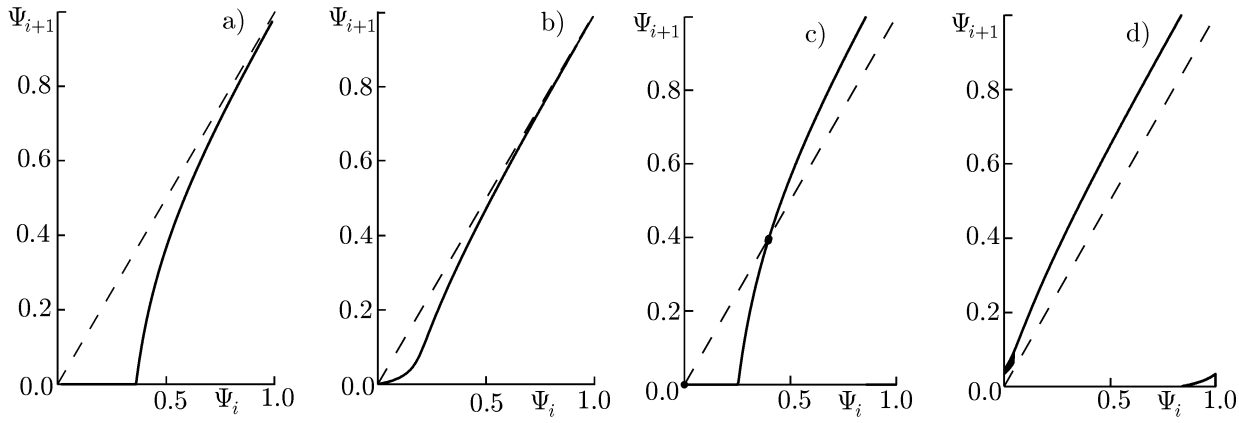

Fig. 8. The first return functions for the phase mapping for the models with fixed (*a* and *b*) and plastic (*c* and *d*) couplings at various parameter space points outside the region $m = 1$ for $A = 2$ mV and $V_{\rm b} = 15.021$ mV: below the lower boundaries of the region $m = 1$ for both models, i.e., $f_{\rm in} = 7.77$ Hz (*a* and *b*), and above the upper boundary of the region $m = 1$ for the model with plastic coupling, i.e., $f_{\rm in} = 9.07$ Hz (*c* and *d*).

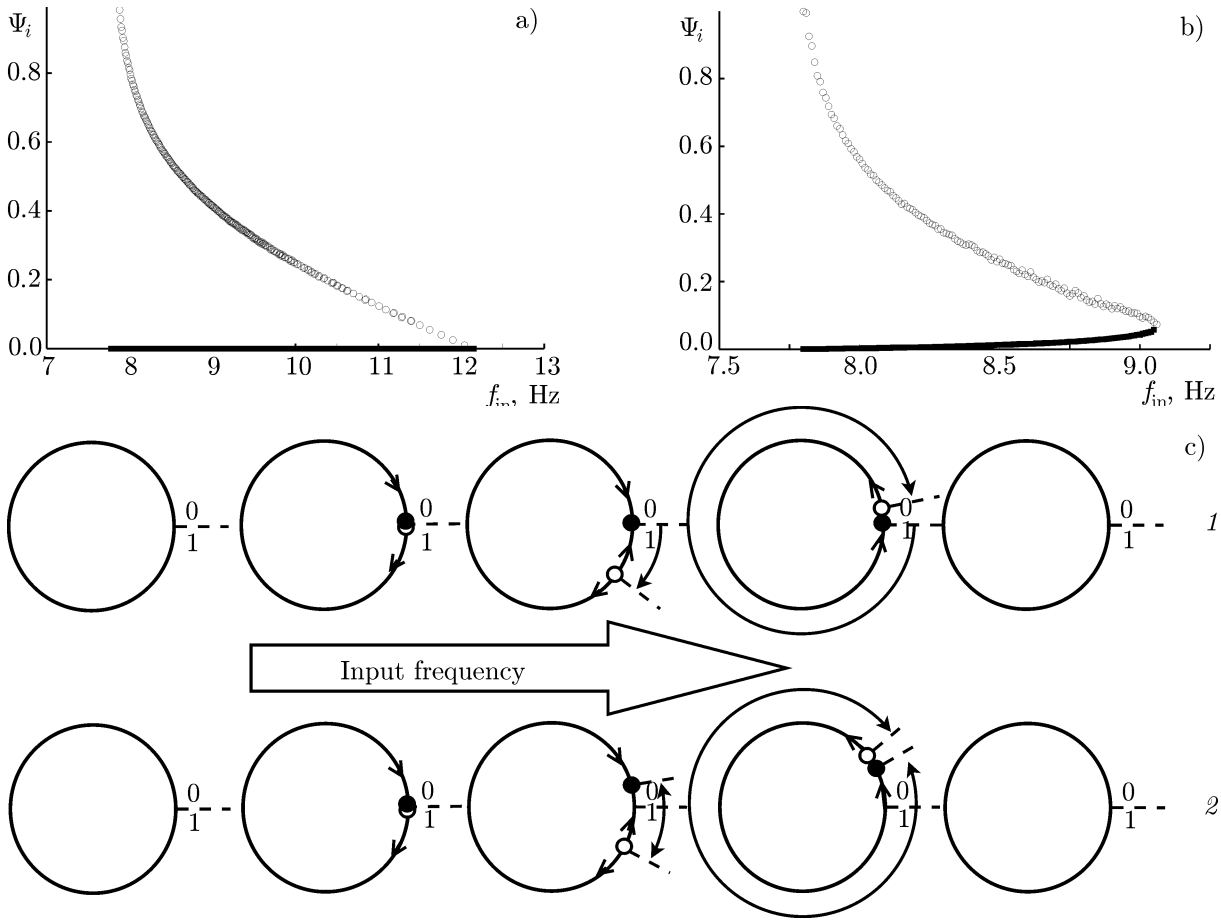

Fig. 9. Bifurcation diagrams for the fixed points of the phase mapping in the frequency range that covers the locking region $m = 1$ ($A = 2$ mV and $V_{\rm b} = 15.021$ mV) for the model with fixed (*a*) and frequency-dependent plastic (*b*) couplings. The bifurcation diagram on the circumference in the frequency range covering the locking region (*c*) for the model with fixed (*1*) and frequency-dependent plastic (*2*) couplings. The open circles and the close squares on panels (*a*) and (*b*) correspond to unstable and stable fixed points, respectively.

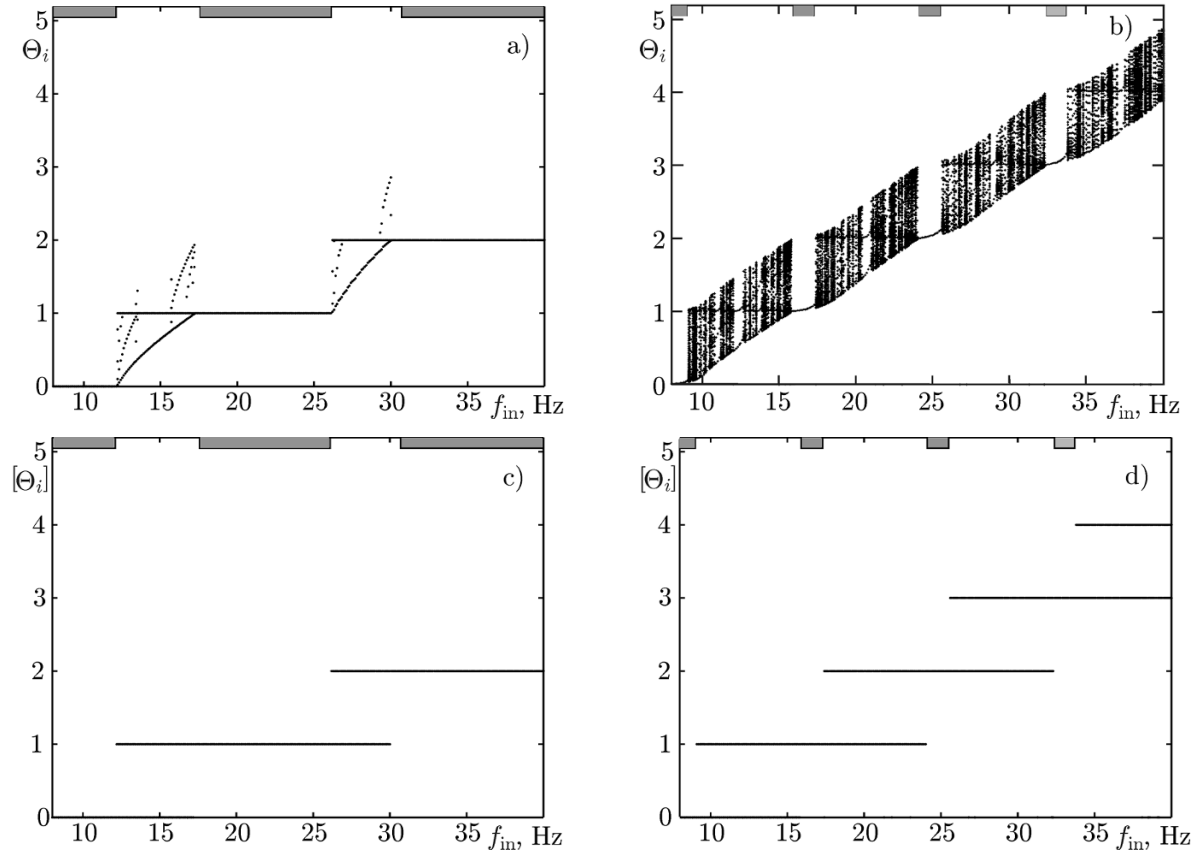

Fig. 10. Bifurcation diagrams of the phase parameter Θ for $A = 2$ mV and $V_{\text{b}} = 15.021$ mV for a model with fixed (*a* and *b*) and frequency-dependent plastic (*c* and *d*) couplings. The rectangular marks in the upper parts of the figures indicate the synchronization regions.

4. CONCLUSIONS

The effects of synchronization of the pulse signals in the model of two interacting neurons with plastic synaptic coupling have been studied compared with the classical case of dynamics of a neural oscillator under the action of a pulse periodic external force. The coupling plasticity in the model is the coupling-force dependence on the frequency of signals of the transmitting neural oscillator. The study has shown that the oscillator synchronization including that at the multiple frequencies is possible in the case of both fixed and plastic couplings. The synchronization regions, which are the Arnold tongues, have been obtained. It is noteworthy that the presence of the frequency-dependent coupling significantly narrows the phase-locking regions and renders the dynamics more regular. In particular, according to Fig. 2*b*, for the fixed frequency of the input signal, the locking regions with various multiple frequencies do not overlap and ensure a regular response with an almost constant locked-phase value for a certain coupling force (see Figs. 10 and 11). In addition, from the viewpoint of neurodynamics, the locking-region narrowing for the plastic coupling can be interpreted as an increase in the frequency selectivity of the neuron response to the external sensor signal. We also note that the plasticity effect (dynamical weakening of the coupling with increasing frequency) makes the oscillator synchronization impossible in the high-frequency region. For the neural systems, this can be interpreted as appearance of homeostatic regulation, i.e., prevention from neuron hyperexcitation during the high-frequency signal generation.

This work was supported by the Russian Foundation for Basic Research (project Nos. 13–02–01223 and 13–04–12041).

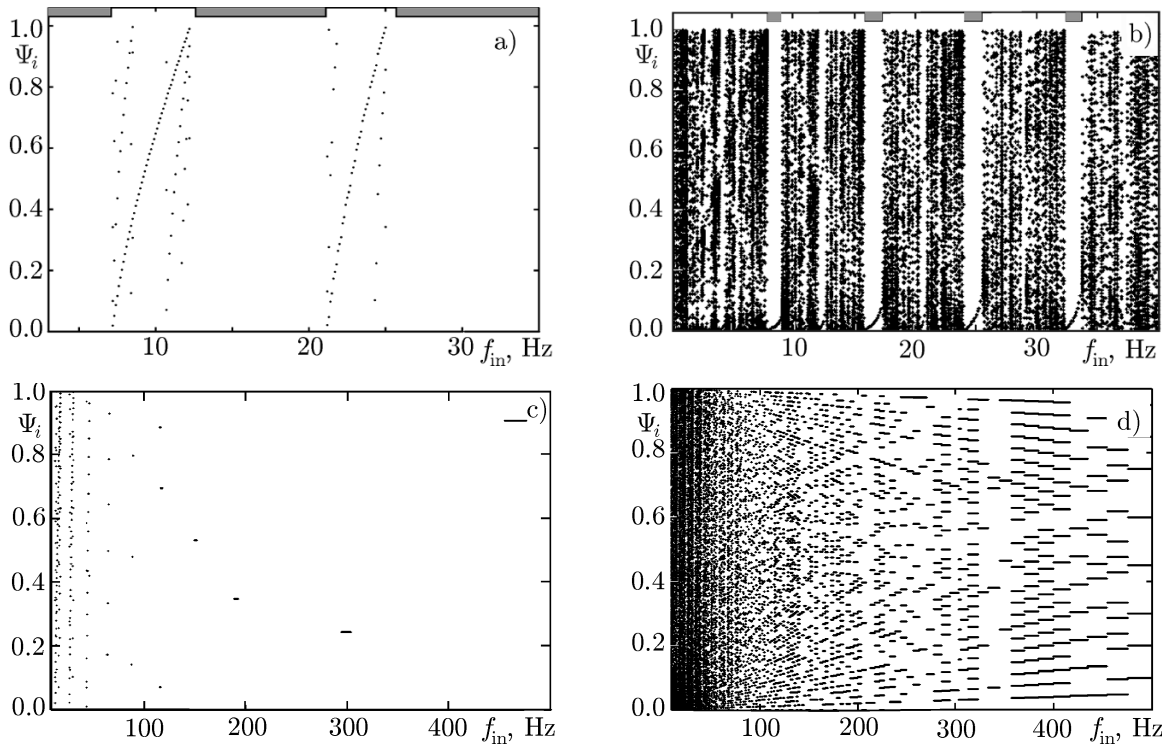

Fig. 11. Bifurcation diagrams of the phase Ψ_i for the model with fixed (*a* and *c*) and frequency-dependent plastic (*b* and *d*) couplings. The rectangular marks in the upper part of panels *a* and *b* denote the synchronization regions. The parameters are equal to $A = 2$ mV and $V_{\text{b}} = 15.021$ mV.

REFERENCES

1. E. M. Izhikevich and G. M. Edelman, *Proc. Nat. Acad. Sci.*, **105**, No. 9, 3593 (2008).
2. V. B. Kazantsev, V. I. Nekorkin, D. V. Artyuhin, and M. G. Velarde, *Phys. Rev. E*, **63**, No. 1, 1 (2000).
3. Q. R. Quian, T. Kreuz, and P. Grassberger, *Phys. Rev. E*, **66**, No. 4, 041904 (2002).
4. V. I. Nekorkin, V. B. Kazantsev, and M. G. Velarde, *Physica D*, **151**, No. 1, 1 (2001).
5. M. Diesmann, M. O. Gewaltig, and A. Aertsen, *Nature*, **402**, No. 6761, 529 (1999).
6. E. M. Izhikevich, *Dynamical Systems*, MIT Press, Cambridge, Mass. (2007), Ch. 10, p. 443.
7. E. Yu. Sitnikova, A. A. Koronovskii, and A. E. Khramov, *Izv. Vyssh. Uchebn. Zaved., Prikl. Nelin. Din.*, **19**, No. 6, 173 (2011).
8. A. A. Koronovskii, and A. E. Khramov, *Izv. Vyssh. Uchebn. Zaved., Prikl. Nelin. Din.*, **19**, No. 4, 91 (2011).
9. A. A. Koronovskii, G. van Luijtelaar, A. A. Ovchinnikov, et al., *Izv. Vyssh. Uchebn. Zaved., Prikl. Nelin. Din.*, **19**, No. 1, 86 (2011).
10. E. Ullner, A. Zaikin, J. García-Ojalvo, and J. Kurths, *Phys. Rev. Lett.*, **91**, No. 18, 180601 (2003).
11. A. Neiman, A. Silchenko, V. Anishchenko, and L. Schimansky-Geier, *Phys. Rev. E*, **58**, No. 6, 7118 (1998).
12. T. Yanagita, T. Ichinomiya, and Y. Oyama, *Phys. Rev. E*, **72**, No. 5, 056218 (2005).
13. H. D. Abarbanel, M. I. Rabinovich, A. Selverston, et al., *Physics — Uspekhi*, **166**, No. 4, 337 (1996).
14. E. Izhikevich, *Int. J. Bifur. Chaos*, **10**, No. 6, 1171 (2000).

15. M. R. Guevara, L. Glass, M. C. Mackey, and A. Shrier, *IEEE Trans. Syst., Man, Cybern.*, **13**, No. 5, 790 (1983).
16. X. Wang, in: *Proc. 1992 IEEE Int. Joint Conf. Neural Networks*, 1992, Vol. 3, p. 517.
17. M. Steriade, D. McCormick, and T. Sejnowski, *Science*, **262**, 679 (1993).
18. W. Klimesch, *Int. J. Psychophysiol.*, **24**, Nos. 1–2, 61 (1996).
19. E. Rodriguez, N. George, and J. Lachaux, *Nature*, **397**, 430 (1999).
20. R. D. Srinivasan, P. Russell, G. M. Edelman, and G. Tononi, *J. Neurosci.*, **19**, No. 13, 5435 (1999).
21. P. Fries, P. R. Roelfsema, A. K. Engel, et al., *Proc. Nat. Acad. Sci.*, **94**, No. 23, 12699 (1997).
22. P. Fries, *Trends Cognitive Sci.*, **9**, No. 10, 474 (2005).
23. J. Fell and N. Axmacher, *Nature Rev. Neurosci.*, **12**, No. 2, 105 (2011).
24. A. Schnitzler and J. Gross, *Nature Rev. Neurosci.*, **6**, No. 4, 285 (2005).
25. I. S. Prokin and V. B. Kazantsev, *Radiophys. Quantum Electron.*, **54**, No. 11, 763 (2011).
26. M. L. Lapicque, *J. Physiol. Patholog. Gen.*, **9**, 620 (1907).
27. M. Tsodyks, A. Uziel, and H. Markram, *J. Neurosci.*, **20**, No. 1, RC50 (2000).
28. A. Katok and B. Hasselblatt, *Introduction to the Modern Theory of Dynamical Systems*, Cambridge Univ. Press, Cambridge (1996).
29. A. Balanov, N. Janson, D. Postnov, and O. Sosnovtseva, *Synchronization: from Simple to Complex*, Springer, New York (2010).
30. A. Pikovsky, M. Rosenblum, and J. Kurths, *Synchronization: a Universal Concept in Nonlinear Sciences*, Cambridge Univ. Press, Cambridge (2003).
31. J. M. T. Thompson and H. B. Stewart, *Nonlinear Dynamics and Chaos*, Wiley, New York (2002).
32. R. Mirollo and S. Strogatz, *SIAM J. Appl. Math.*, **50**, No. 6, 1645 (1990).